HERON is jointly edited by:
STEVIN-LABORATORY of the department of Civil Engineering, Delft University of Technology, Delft, The Netherlands
and
INSTITUTE TNO for Building Materials and Building Structures. Rijswijk (ZH), The Netherlands.
HERON contains contributions based mainly on research work performed in these laboratories on strength of materials, structures and materials science.

Secretary:
G. J. van Alphen
Stevinweg 1
P.O. Box 5048
2600 GA Delft, The Netherlands
Tel. 0031-15-785919
Telex 38070 BITHD

HERON vol. 26 1981 no. 4

Contents

TESTING OF FOUNDATION PILES

H. van Koten and P. Middendorp

IBBC-TNO
Institute for Building Materials and Building Structures
Lange Kleiweg 5, Rijswijk, The Netherlands

Testing of foundation piles

1 General introduction

Due to the development of heavy structures and high-rise buildings in the last decades, the application of foundation piles in areas with soft upper strata has increased considerably.

The quality of the foundation is one of the most important factors that determine the safety and overall stability of a structure.

That is why the Institute TNO for Building Materials and Building Structures has developed two methods based on stress wave analysis, which enable the quality of a pile foundation to be determined quickly, economically and reliably.

The first method, called integrity testing, provides information on pile length, deformations, cracks and other discontinuities.

Furthermore, the severity and the location of a discontinuity can be determined.

The second method, called the (dynamic) bearing capacity test, is concerned with the prediction of the bearing capacity of a pile in terms of toe resistance, skin friction and settlement under static loading.

Testing all piles by means of the integrity test gives a good idea of the "integrity" quality of a pile foundation.

2 Integrity tests

2.1 *Introduction*

The integrity test is a simple test offering the possibility of determining the shape, the length and discontinuities in foundation piles in the ground.

The test consists of delivering a blow with a hammer on top of the pile, while the response of the pile is measured with an accelerometer.

The test result is made visible on an oscilloscope and can be analysed immediately.

The analysis has been made easy by transforming the acceleration into a signal with clear information about the discontinuities at lower levels in the piles.

2.2 *Integrity testing equipment*

The integrity testing equipment (Fig. 1) consists of an oscilloscope connected to signal convertor.

An accelerometer, pressed by hand on the pile top (Fig. 2) records the movement due to a hammer blow.

The accelerometer is placed near the point of impact where the pile is struck.

A normal measurement result represents the one time integrated acceleration signal.

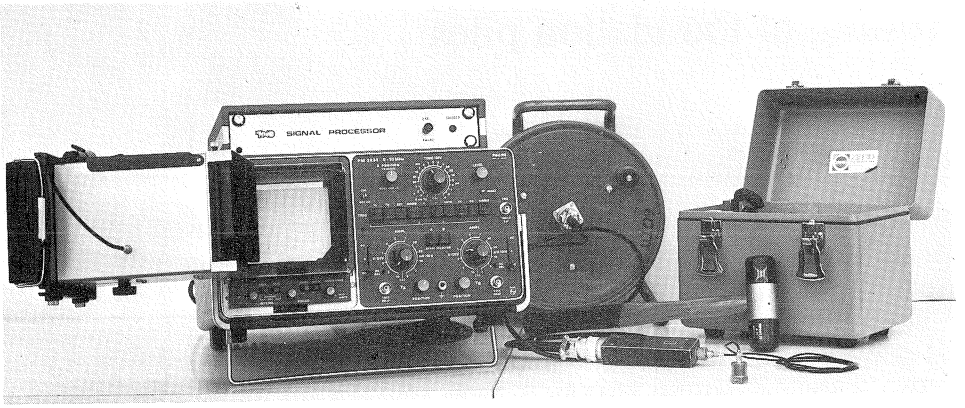

Fig. 1. Integrity test equipment.

Fig. 2.
Integrity testing.

So it represents a velocity of the pile top and appears on the oscilloscope screen as a straight line with two dips.

One dip is caused by the pile movement due to the blow and the other dip by the reflex from the toe (see Fig. 3).

Amplification of the signal with increasing time reveals the reflex from the toe more clearly.

The properties of the accelerometer applied and manner of integration cause a reduction of lower frequencies in the signal. All modifications of the signal result in almost

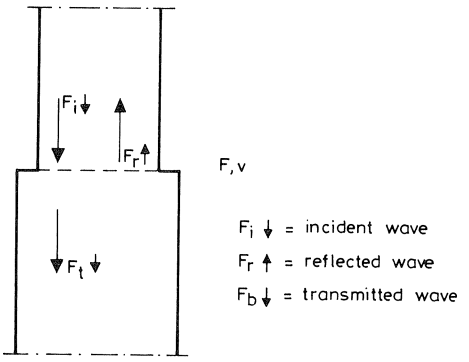

Fig. 3. Waves in a pile with a discontinuity.

straight parallel lines on the screen. In most cases the measurement on a pile is repeated four or five times to eliminate possible electric disturbances.

The complete integrity test equipment is portable and can be transported in an ordinary private car.

A test with this battery-equipped apparatus takes only a few minutes, so that up to two hundred foundation piles can be tested in one day.

2.3 *Some theoretical aspects*

The solution of the wave equation (see for example [8]) indicates that if a force F is introduced into a pile, two waves are generated wich are propagated with a velocity:

$$c = \sqrt{\frac{E}{\rho}} \tag{1}$$

where:

E = modulus of elasticity
ρ = density of pile material

One wave indicated by $F\downarrow$ travels to the pile toe, the other wave $F\uparrow$ in the opposite direction.

For a pile without skin friction the wave forces are related to the velocities in the wave as follows:

$$v\downarrow = F\downarrow / Z \tag{2}$$

$$v\uparrow = -F\uparrow / Z \tag{3}$$

where Z represents the impedance of the pile:

$$Z = EA/c \tag{4}$$

A = cross section of the pile

The velocity of a material particle in the pile at a certain level is determined by the sum of the arriving waves at that level:

$$v = v\downarrow + v\uparrow \tag{5}$$

The force acting on a particle is:

$$F = F\downarrow + F\uparrow \tag{6}$$

If a force F_i is introduced into the top of the pile by a blow from a hammer, a stress wave $F_i\downarrow$ will start to travel to the toe:

$$F_i\downarrow = F_i \tag{7}$$

$$F_i\uparrow = 0 \tag{8}$$

Let the impedance of the pile be Z_1; it follows for the particle velocities in the wave that:

$$v_i\downarrow = v_i = F_i/Z_1 \tag{9}$$

$$v_i\uparrow = 0 \tag{10}$$

If the pile has a discontinuity with impedance Z_2, the wave $F_i\downarrow$ will be partly reflected.

From the condition that at the transition of impedance v and F must be equal for both pile parts the reflected force $F_r\uparrow$ can be deduced (see Fig. 3). F_r and F_t are values for the transmitted wave; hence:

$$F = F\downarrow + F_r\uparrow = F_t\downarrow \tag{11}$$

$$v = v\downarrow + v\uparrow = v_t\downarrow \tag{12}$$

Substituting (2), (3) and (12) into (11) yields

$$F_r\uparrow = \frac{Z_2 - Z_1}{Z_2 + Z_1} F_i\downarrow \tag{13}$$

or

$$v_r\uparrow = \frac{Z_1 - Z_2}{Z_1 + Z_2} v_i\downarrow \tag{14}$$

The reflected wave $F_r\uparrow$ travels back to the top of the pile.

At the moment of arrival of the wave $F_r\uparrow$ the force F_p acting on the top is zero:

$$F_p = 0 \tag{15}$$

$$F_p\uparrow = F_p\downarrow = 0 \tag{16}$$

$$F_p\uparrow = F_p\downarrow = F_r\uparrow \tag{17}$$

Introducing (2) and (3) yields:

$$v_p\uparrow = -F_r\uparrow/Z_1 \tag{18}$$

$$v_p\downarrow = -F_r\uparrow/Z_1 \tag{19}$$

So the particle velocity v_p at the top due to a reflected wave is:

$$v_p = v\uparrow + v\downarrow = \frac{-2F_i\uparrow}{Z_1} = 2v_i\uparrow \tag{20}$$

The above formulas can also be derived by using the force-velocity diagram (see Fig. 4) based on the method of characteristics [3].

The quotient r of the initial particle velocity v_i at the top of the pile due to a hammer blow and the particle velocity due to the reflected wave v_p can be used to calculate the dimensions of a change in cross-section A_2:

$$r = \frac{v_p}{v_i} = \frac{2v_r\uparrow}{v_i\downarrow} \tag{21}$$

Substituting (14) and taking into account that E and c are constants for a homogeneous pile, we obtain:

$$\frac{A_2}{A_1} = \frac{2-r}{2+r} \tag{22}$$

This relation has been plotted in Fig. 5.

In a cylindrical pile the wave $F_i\downarrow$ travels without interruption to the pile toe and reflects partly as a wave $F_r\uparrow$.

The arriving reflected waves from dicontinuities and pile toe are recorded by an accelerometer.

Fig. 6 represents the one time integrated accelerometer signal measured at the top of a cylindrical pile in the soil.

The maximum velocity of the particles at the top caused by a hammer below is about 11×10^{-3} m/s.

This velocity is considerably reduced by the skin friction along the pile shaft.

The influence of the skin friction on the initial velocity v_i can be expressed as [2]:

$$v_r = v_i e^{-\alpha t} \tag{23}$$

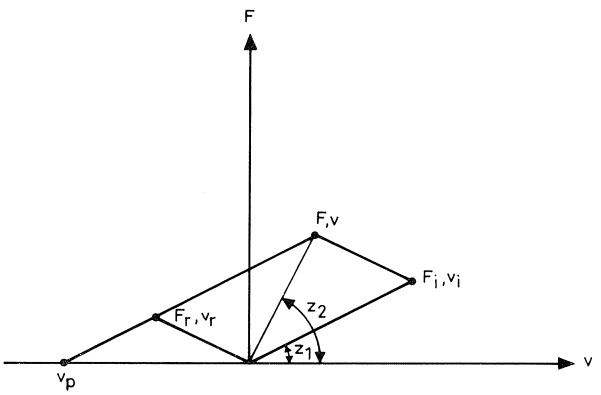

Fig. 4. Force-velocity diagram.

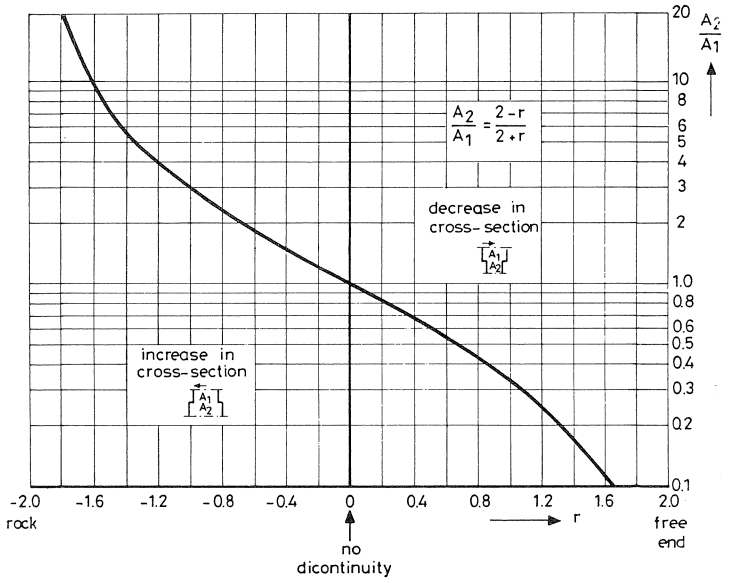

Fig. 5. Relation between reflection coefficient r and change in cross-section A_2/A_1.

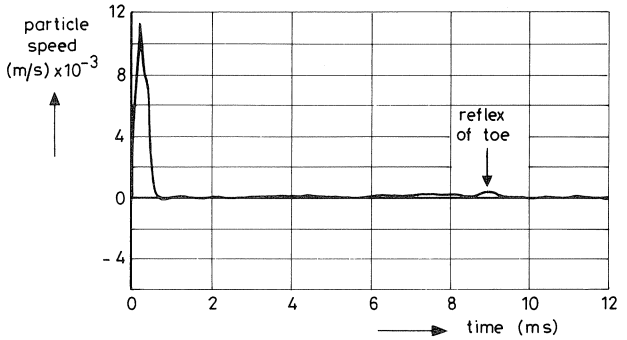

Fig. 6. Measured particle velocity at pile after a blow with a hammer.

where:

v_r = reduced velocity
α = damping factor
t = time

By multiplying the measured velocity by the amplification defined as:

$$a = e^{\alpha t} \tag{24}$$

the reduction of the signal due to skin friction can be eliminated.

If the factor α is suitably chosen, the measured velocity can be used to calculate the dimensions of the discontinuities in a pile.

2.4 *Interpretation of integrity test results*

In this section some basic cases of integrity test results will be considered.

They can be distinguished as follows:
- a pile standing on rock
- a pile with a free end
- a pile with an increase in cross-section
- a pile with a decrease in cross-section
- a fractured pile

In the treatment of these cases it is assumed that the reduction of reflected waves due to skin friction is eliminated by the built-in amplification of the integrity test device.

Pile standing on rock

Fig. 7 represents a velocity-time diagram for the particle velocity at the pile top and a depth-time diagram from which the position of a stress wave in a pile can be read.

At the time $t = 0$ a blow is delivered upon the pile and results in a compression wave $F_i \downarrow = F_i$ with a particle velocity $v_i \downarrow = v_i$ travelling to the pile toe.

If L is the pile length, the wave reaches the toe after a time $t = L/c$.

For a pile standing on rock it can be assumed that the particle velocity at the toe $v = 0$.

From this condition and equations (3) and (6) it follows for the reflected wave travelling upwards that:

$$v_r \uparrow = -v_i \downarrow = -v_i \tag{25}$$

$$F_r \uparrow = F_i \downarrow = F_i \tag{26}$$

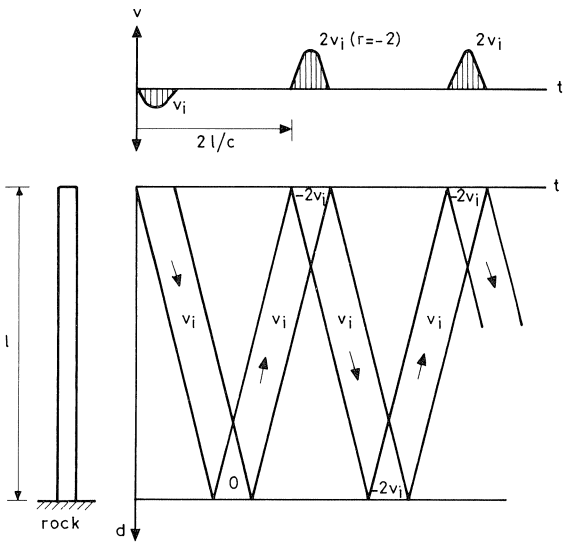

Fig. 7. Pile standing on rock.

The particle velocity in the reflected wave is in opposition to that of the initial wave. So the pile will jump up.

The stress in the reflected wave remains compressive stress.

After a time $2L/c$ the reflected wave can be seen at the pile top. The recorded particle velocity is $v_p = 2v_i$ because of the free end condition.

Pile with free end

In this case the condition at the toe is:

$$F = 0$$

Now it follows from equations (5) and (6) for the reflected wave that:

$$v_r \uparrow = v_i \downarrow = v_i \tag{27}$$

$$F_r \uparrow = -F_i \downarrow = -F_i \tag{28}$$

The particle velocity in the reflected wave remains the same as in the initial wave. So the pile will move downwards.

The stress in the reflected wave is of opposite sign and changes into tension (see Fig. 8). The reflected wave can be seen at the pile top after a time $2L/c$, where it causes a particle velocity $v_p = 2v_i$.

Fig. 9 shows the measured signals for a pile with a free end.

Pile with increase in cross-section

If the wave travelling downwards initiated by the hammer blow meets an increase in cross-section, the particle velocity will be somewhat reduced and will produce a reflected wave (see Fig. 10).

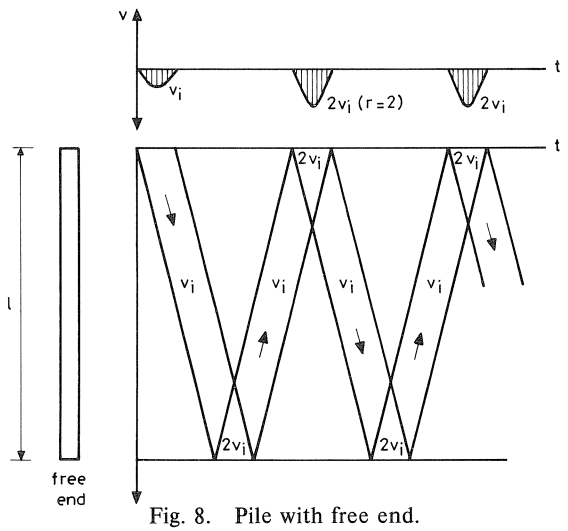

Fig. 8. Pile with free end.

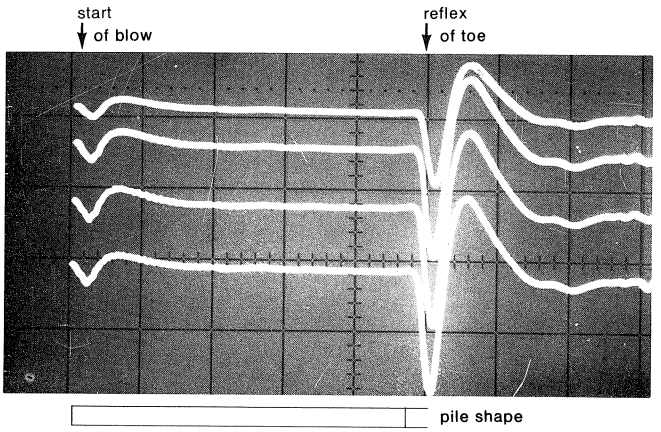

Fig. 9. Measured signals for a pile with free end.

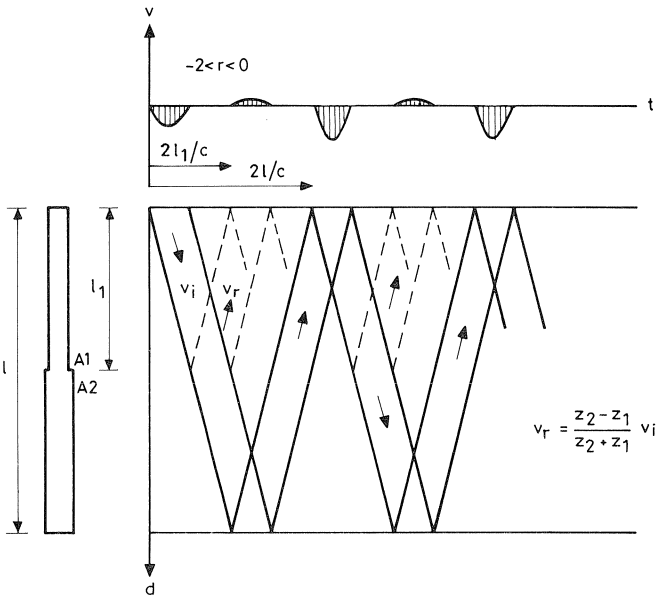

Fig. 10. Pile with increase in cross-section.

The stress in this wave is a compressive stress, just as in the case of the reflected wave from the toe of a pile standing on rock, and the particle velocity is directed upwards.

If L_1 is the level where the increase in cross-section occurs, an extra movement upwards can be seen in the signal recorded at the top after a time $2L_1/c$.

The value of the reflected wave depends on the ratio of impedances given by equations (13) and (14).

Fig. 11 shows the measured signal for a pile with a local increase in cross-section.

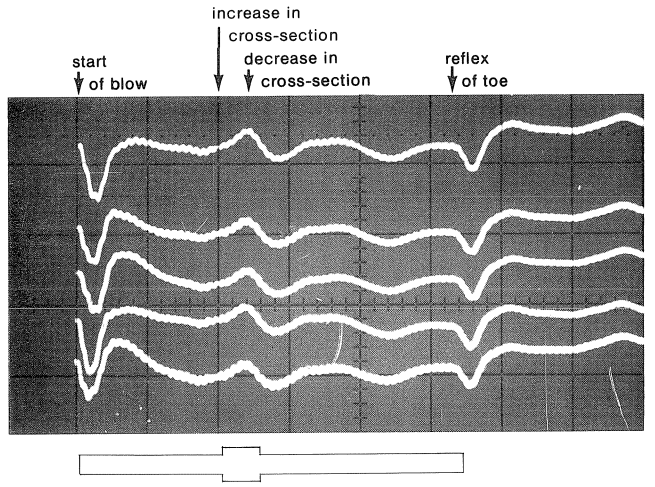

Fig. 11. Measured signals for a pile with a local increase in cross-section.

Pile with decrease in cross-section

At the arrival of a decrease in cross-section the compression wave travelling downwards will meet less resistance (see Fig. 12).

This means that the pile will be subjected to a little tension, and this results in a wave reflected to the pile top.

The stress in this wave is a tensile stress, just as in the case of the reflected wave from the toe of a free pile, and the particle velocity is directed downwards.

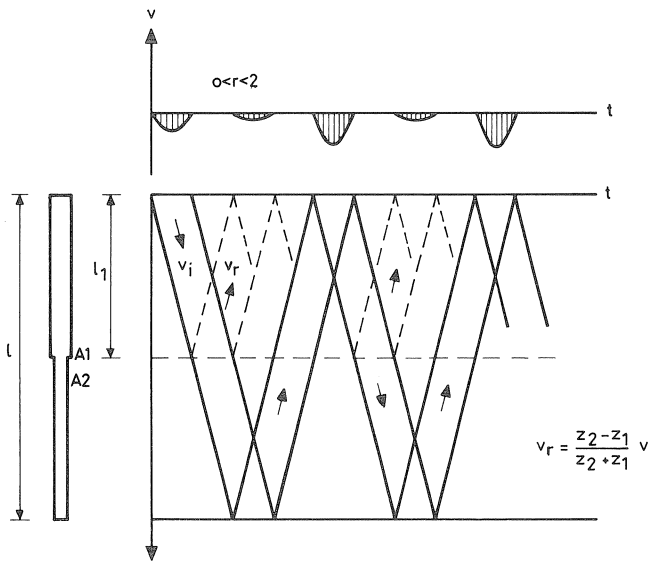

Fig. 12. Pile with decrase in cross-section.

If L_1 is the level where the decrease in cross-section occurs, an extra movement downwards can be seen in the signal recorded at the top after a time $2L_1/c$.

Fig. 13 represents the measured signal for a pile with a local decrease in cross-section.

Fractured pile

A pile fractured at a level L_d from the top behaves like a pile with a free end at that level.

The stress wave is not able to travel to the toe and moves to and fro between the pile top and the fractured zone.

This can be seen in the signals recorded at the pile top by the occurrence of equally spaced dips (see Fig. 14).

The time t_d between the dips determines the depth L_d of the fractured zone:

$$L_d = \frac{ct_d}{2} \tag{29}$$

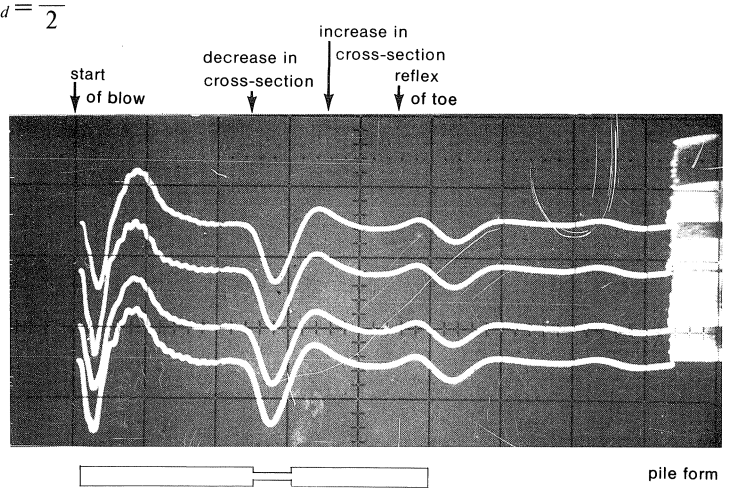

Fig. 13. Measured signals for pile with local decrease in cross section.

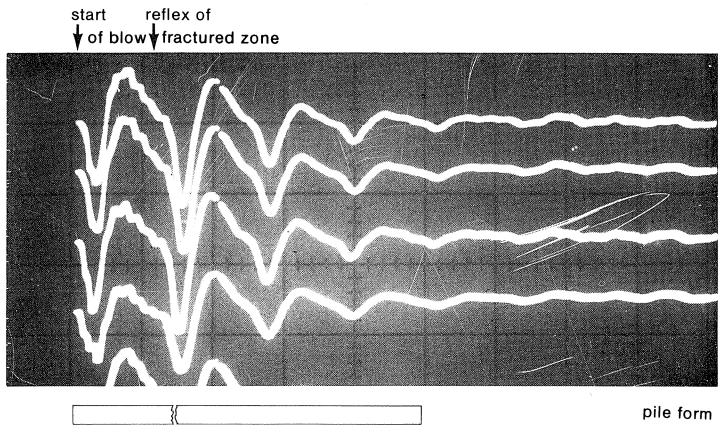

Fig. 14. Measured signals for fractured pile.

General remarks

The cases that have been dealt with here show that discontinuities in a pile can be detected by analysing the particle velocity recorded at the pile top after a hammer blow.

Decreases and increases in cross-section manifest themselves by a downward or upward movement of the pile top.

The location of a discontinuity at a depth L_d can be determined by measuring the time of occurrence t_d of a reflex in the signal (eq. (29)).

In the same manner the length of a pile can be determined by measuring the time of occurrence of a reflex from the pile toe. From the ratio of initial wave and reflected wave the variation of cross-section of a discontinuity can be calculated.

Combining the cases of an increase and a decrease in cross-section enables the length of a variation in cross-section to be determined.

For the case of a cracked zone there is an abrupt change in cross-section.

So a crack will produce a relative sharp reflex, a variation in cross-section yields a more spread-out signal.

3 Bearing capacity test

3.1 *Introduction*

The bearing capacity test is based on the principle of measuring the force and displacement of the pile top during dynamic loading caused by the impact of a heavy drop hammer or an accelerated smaller mass.

Analysis is done by a micro-computer on the site, immediately after testing.

The basic analysis will be explained. It includes the calculation of skin friction, toe resistance, dynamic influences and the prediction of the behaviour of the pile under static loading. One of the sections of this chapter will describe the testing and loading equipment.

In the case histories (Chapter 4) the soil is considered as a velocity-independent ideally plastic material. In other cases the velocity-dependence has to be taken into account.

3.2 *Some theoretical aspects*

If the assumption is made that the impact force acting on the top of the pile is not influenced by skin friction, it is possible to determine the skin friction, toe resistance and spring stiffness of the soil by analysing only the movements of the top of the pile.

An example of such a movement is given in Fig. 15 and presented as a displacement-time diagram.

The information in this curve will be analysed step by step.

The first part of the time-displacement curve ($0 \leq t \leq t_1$) represents settlement due to pressure. The second part ($t_1 \leq t \leq t_2$) is partial destressing due to skin friction.

The downward displacement during the time ($t_2 \leq t \leq t_3$) is caused by the penetration of the toe of the pile into the soil.

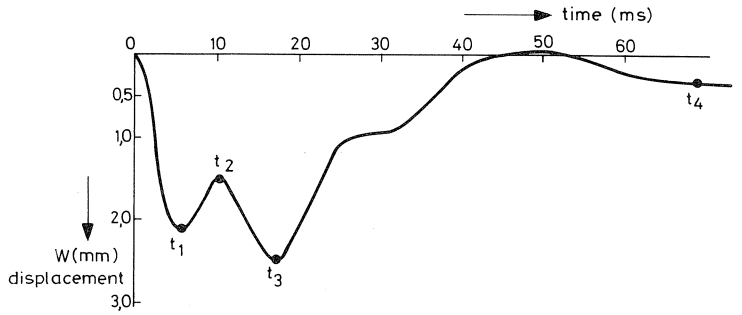

Fig. 15. Time-displacement due to dynamic loading.

Part 4 ($t_3 \leq t \leq t_4$) is the effect of elastic destressing of the soil and the pile. The last part ($t > t_4$) represents the rest of the settlement of the pile after the blow.

These different parts of the time-displacement curve will be discussed in detail.

3.2.1 Part 1 Compression

The displacement of the top of the pile (w) due to compression of a part of the pile under a constant load F is:

$$w = \frac{Fl}{EA} \tag{31}$$

E is the modulus of elasticity; A is the cross-sectional area of the pile shaft. In the expression for w, l is the length of the compressed part of the pile. This length is determined as the product of the time of duration of the impact (t_0) and the velocity of stress waves in the pile (c):

$$l = c \cdot t_0 \tag{32}$$

The value of c follows from:

$$c = \sqrt{\frac{E}{\rho}} \tag{33}$$

for concrete $c = 4000$ m/s $= 4$ m/ms
for steel $c = 5200$ m/s $= 5.2$ m/ms

If the load F is not constant in time, the expression for the displacement becomes:

$$w = \int_0^t \frac{F(t) \cdot c \cdot \mathrm{d}t}{EA} \tag{34}$$

This relation between displacement and force can, after differentiation, be written as:

$$\frac{\mathrm{d}w}{\mathrm{d}t} = v(t) = \frac{F(t) \cdot c}{EA} \quad \text{(basic formula)} \tag{35}$$

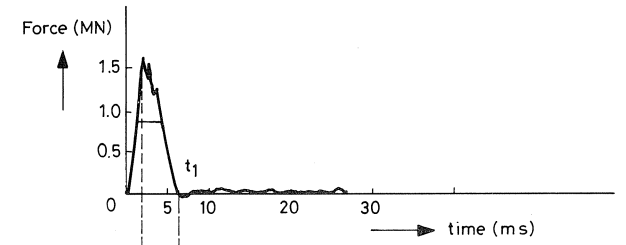

Fig. 16a. The compression force.

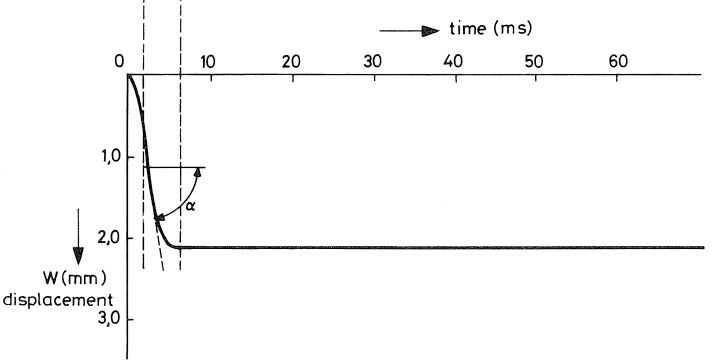

Fig. 16b. Displacement of the top of an infinitely long pile.

With this expression the force $F(t)$ can be derived from the first part of the time-displacement curve in Fig. 15.

The factor EA/c is called the impedance of the pile.

The result of such a calculation is given in Fig. 16a. The displacement of the top of an infinitely long pile caused by the force is given in Fig. 16b.

The displacement remains constant after the blow while the stress wave goes into the pile.

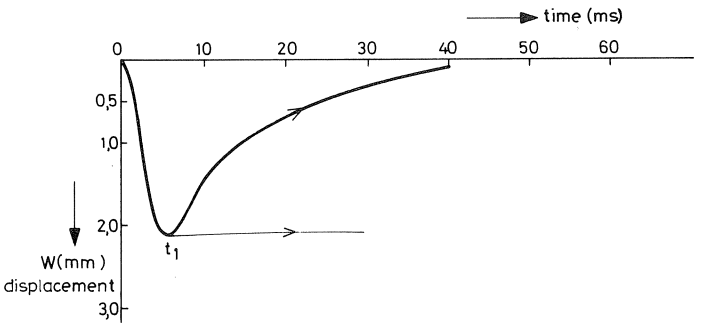

Fig. 17. Influence of skin friction on the displacement of the top of an infinitely long pile.

3.2.2 Part 2 Skin friction

In the case of skin friction the displacment at the top is no longer constant, but decreases as indicated in Fig. 17.

The constant displacement of the top of the pile is influenced by the skin friction. The displacement and the stress wave are reduced by this friction.

The magnitude of the skin friction can be determined by differentiation (see the basic formula). The skin friction can be influenced by dynamic forces, e.g., in the case of clay layers. The elimination of dynamic forces, in order to obtain the static component of the skin friction will be treated in another section.

3.2.3 Part 3 Soil penetration

The movement of the top of a pile of finite length without skin friction and without resistance at the toe is given in Fig. 18.

The first part is again the compression, and after the constant displacement the return of the stress wave from the toe of the pile can be seen.

The displacement of a pile without skin friction, but with some resistance at the toe, is represented by the dotted line in Fig. 18. The reflected stress wave is reduced by the toe resistance.

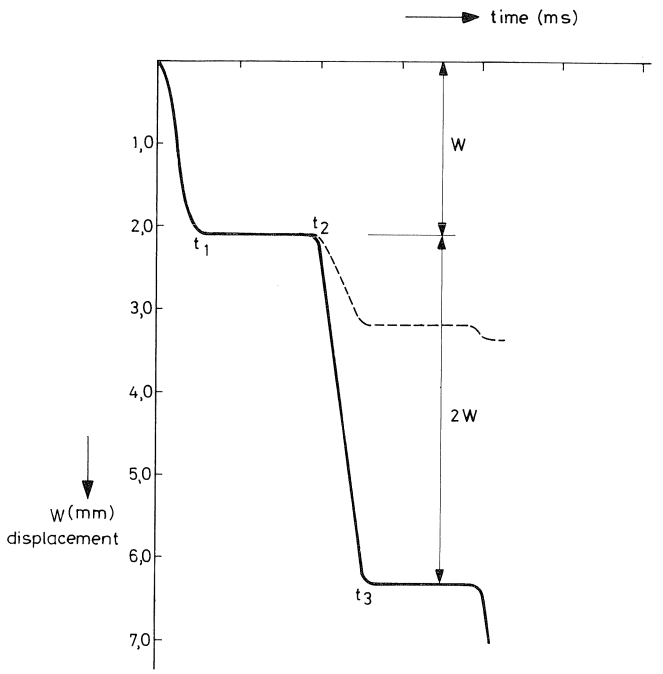

Fig. 18. Displacement of the top of a pile with finite length in the absence of skin friction and toe resistance.
Dotted line: same case, but there is some resistance at the toe of the pile.

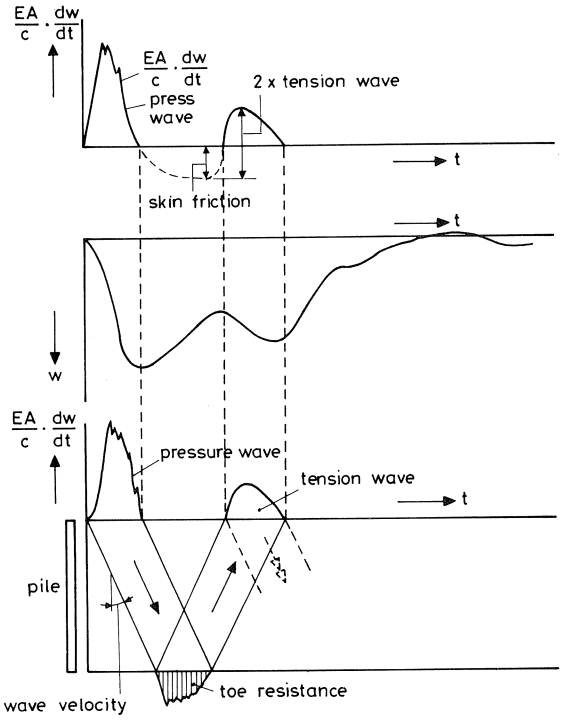

Fig. 19. Displacement of the top of a pile when skin friction and toe resistance are present.

The magnitude of the reflected wave is found by differentiation of the displacement (see again the basic formula).

From the difference between the impact force and the reflected wave the toe resistance can be calculated. In this case, too, the toe resistance may by influenced by dynamic forces, which have to be eliminated to obtain the static toe resistance.

The analysis of the measured displacement of the top of a pile in the case of skin friction and toe resistance is presented schematically in Fig. 19.

3.2.4 Part 4 Destressing

Part 4 of the time-displacement curve demonstrates the elastic destressing of the pile and soil after the blow.

In this part of the signal the stress wave is almost damped out.

The movement approximately conforms to the theory of a damped single-freedom system, which is described by the following differential equation:

$$M\frac{d^2w}{dt^2}+C\frac{dw}{dt}+K_s w=0 \tag{36}$$

where:

M = mass of the pile [kg]
C = damping of the soil [Ns/m]
K_s = spring stiffness of the soil [N/m]

Because the acceleration, velocity and displacement are known at every instant, the damping and spring stiffness of the soil can be calculated.

3.2.5 Part 5 Remaining settlement

The last part of the signal represents the remaining settlement and serves as a criterion for the attainment of the ultimate bearing capacity of a foundation pile.

Up to now this criterion has been an empirical value. An improvement will be obtained if local soil conditions and the characteristics of the pile are taken in account.

3.3 Calculation of static pile behaviour from dynamic bearing capacity

The evaluation of dynamic test results can be summarized as follows. As appears from the formula:

$$F = \frac{EA}{c}\frac{\mathrm{d}w}{\mathrm{d}t} \tag{37}$$

the gradient of the time-displacement curve characterizes the forces acting on the pile.

The impact load is determined by the angle α, the skin friction by β, and the toe resistance by γ (see Fig. 20).

The spring stiffness of the pile and soil can be calculated from the destressing part of the signal.

The remaining settlement w_r is a criterion for the attainment of the ultimate bearing capacity of a pile.

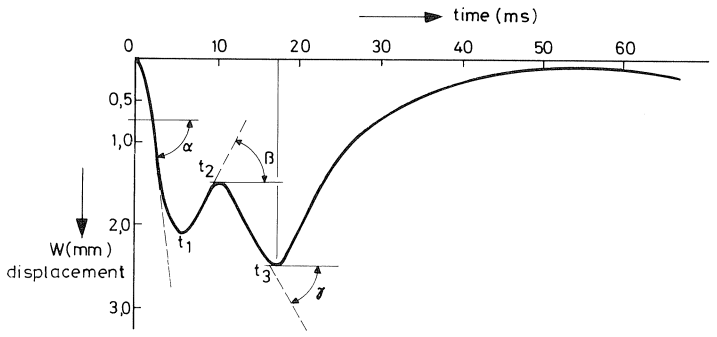

Fig. 20. The angles α, β and γ determine the load, the skin friction and the toe resistance. respectively.

The influence of clay strata

As already mentioned earlier on, the measured skin friction toe resistance may be influenced by dynamic properties of the soil, which have to be eliminated to obtain the skin friction and toe resistance for the static case.

Heerema [4], Dayal and Allen [1], and Poskitt [6] indicate that in the case of clay strata the measured skin friction and toe resistance are velocity-dependent.

The dynamic part of the skin friction and toe resistance is eliminated as follows:

$$q_s = \frac{1}{1 + K_L \log \frac{V_d}{V_s}} \cdot q_d \tag{38}$$

where:

q_s = static toe resistance or skin friction
q_d = dynamic toe resistance or skin friction
V_d = penetration velocity during the dynamic bearing capacity test
V_s = penetration velocity during the static bearing capacity test
K_L = soil viscosity coefficient

The coefficient K_L has to be determined for each soil stratum that contributes velocity-dependent forces during the dynamic bearing capacity test.

The load-displacement diagram

When the dynamic properties of clay at the skin and the toe have been eliminated, the sum of these two quantities yields the failure load (F_f) of the pile for the static case. The failure load is defined as the asymptote of the load-displacement diagram.

With the information now obtained it is possible to estimate the static load behaviour of the pile.

It has been shown by Rollberg [7] that a good fit for the first part of a static load diagram is given by a hyperbola of the form:

$$s = \frac{aF}{1 - bF} \tag{39}$$

where:

s = settlement
F = load
a = 1/K

For K the spring stiffnesses of the pile (K_p) and soil (K_s) are adopted.

$$b = \frac{1}{F_f} \tag{40}$$

$F_f = F_s + F_t$ = failure load
F_s = skin friction
F_t = toe resistance

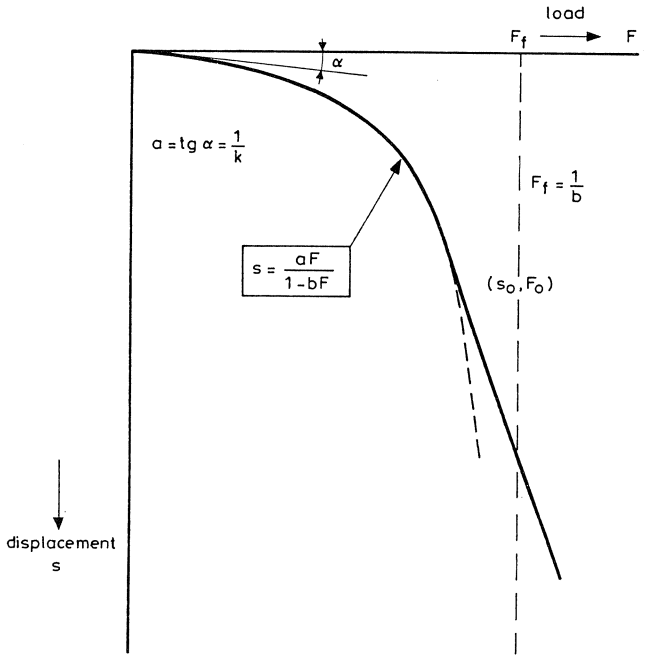

Fig. 21. Load-displacement diagram.

Therefore, with the calculated results F_s, F_t and K the load displacement diagram is fully determined (see Fig. 21).

At an emperical determined settlement s_0 the hyperbola continues into a straight line, which is the tangent in that point.

Examples of predicted load-displacement diagrams will be given in subsequent sections of this report.

3.4 Equipment for bearing capacity tests

3.4.1 *Measuring equipment*

The bearing capacity test is based on the principle of measuring the force and the displacement near the top of a foundation pile, caused by an impact load.

Strain gauges, glued to two opposite sides of the pile near the top (see Fig. 22) measure the force in the pile.

The movement of the top of the pile can be measured with an electronic theodolite, which gives a displacement signal (see Fig. 23), or with an accelerometer.

The theodolite and strain gauges are connected to a signal processor and transmitted to a microcomputer. In principle the signals can be processed immediately, and storage on analogue magnetic tape is not necessary.

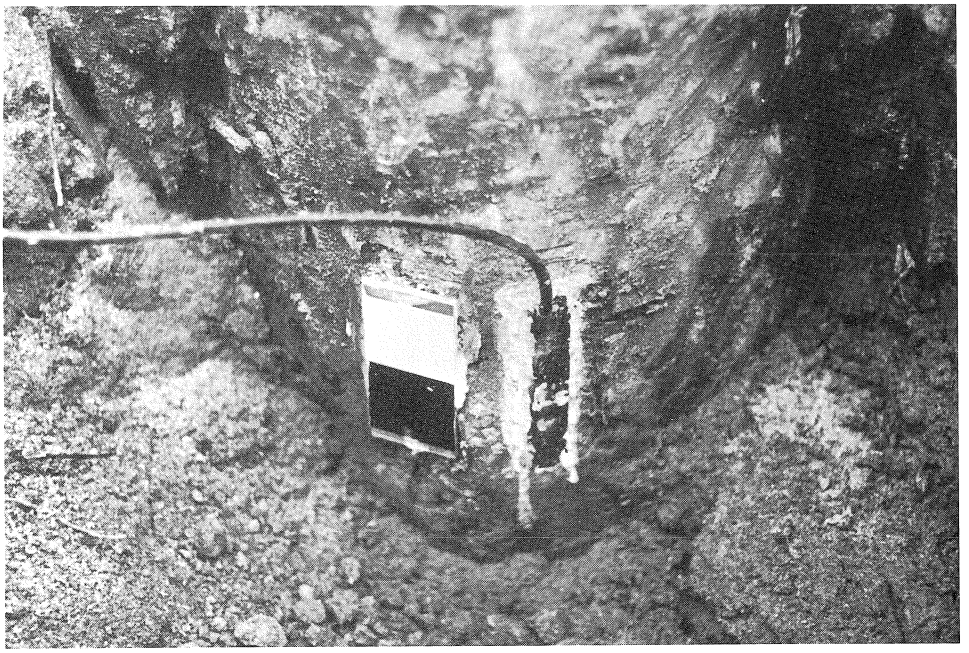

Fig. 22. Black-white spot, strain gauge glued to the pile near the top.

Fig. 23. Electronic theodolite.

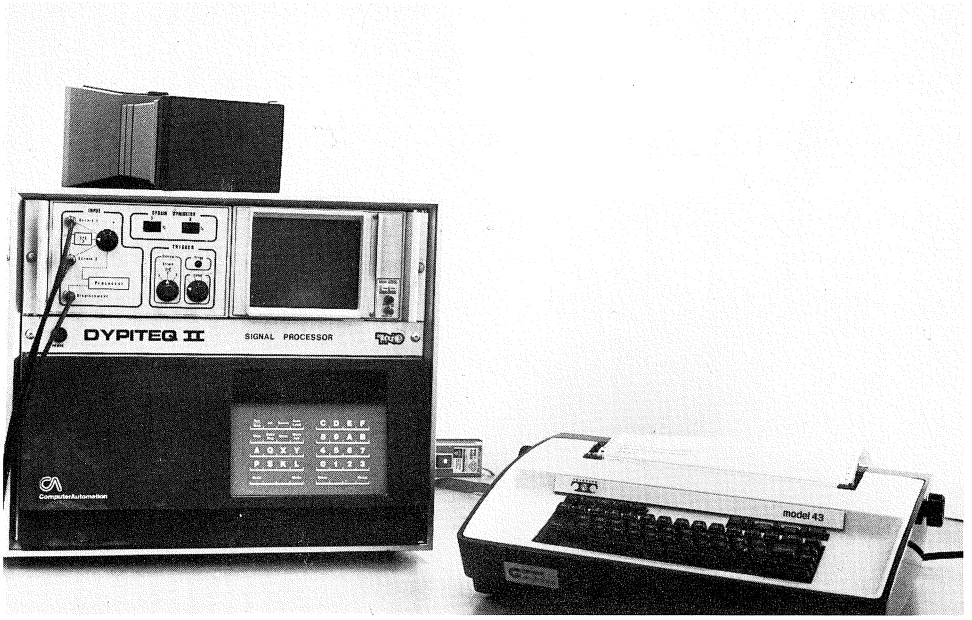

Fig. 24. Microcomputer.

The main part of the TNO equipment for bearing capacity tests is the microcomputer with EPRO memory (see Fig. 24).

Strain and displacement signals are directly analysed with the aid of a computer program. Communication between computer and operator takes place via a teletype system. Operation of the computer is made very simple because it is based on a "question-answer" principle for which no special programming experience is required.

After analysis, the computer plots the test results on an oscilloscope screen. The results are permanently recorded with a Polaroid camera and presented in a report written by the computer on the teletype-writer.

3.4.2 *Loading equipment*

Loading the pile for the bearing capacity test is the most difficult part of the test because a drop-weight and a crane are needed.

Drop-weights (see Fig. 25) ranging from 800–2000 kg are normally used.

For special circumstances, e.g., if no crane is available, TNO has developed a "portable" pneumatic hammer (see Fig. 26).

In this case the pile is loaded by a pneumatically accelerated mass of 100 kg. The system has been based on the principle that the mass acts as a piston, which is connected to an air pressure chamber by means of an anchor bolt.

The anchor bolt has been so designed that it collapses at a certain ajustable air pressure. The piston then moves downwards and strikes the pile top at high velocity.

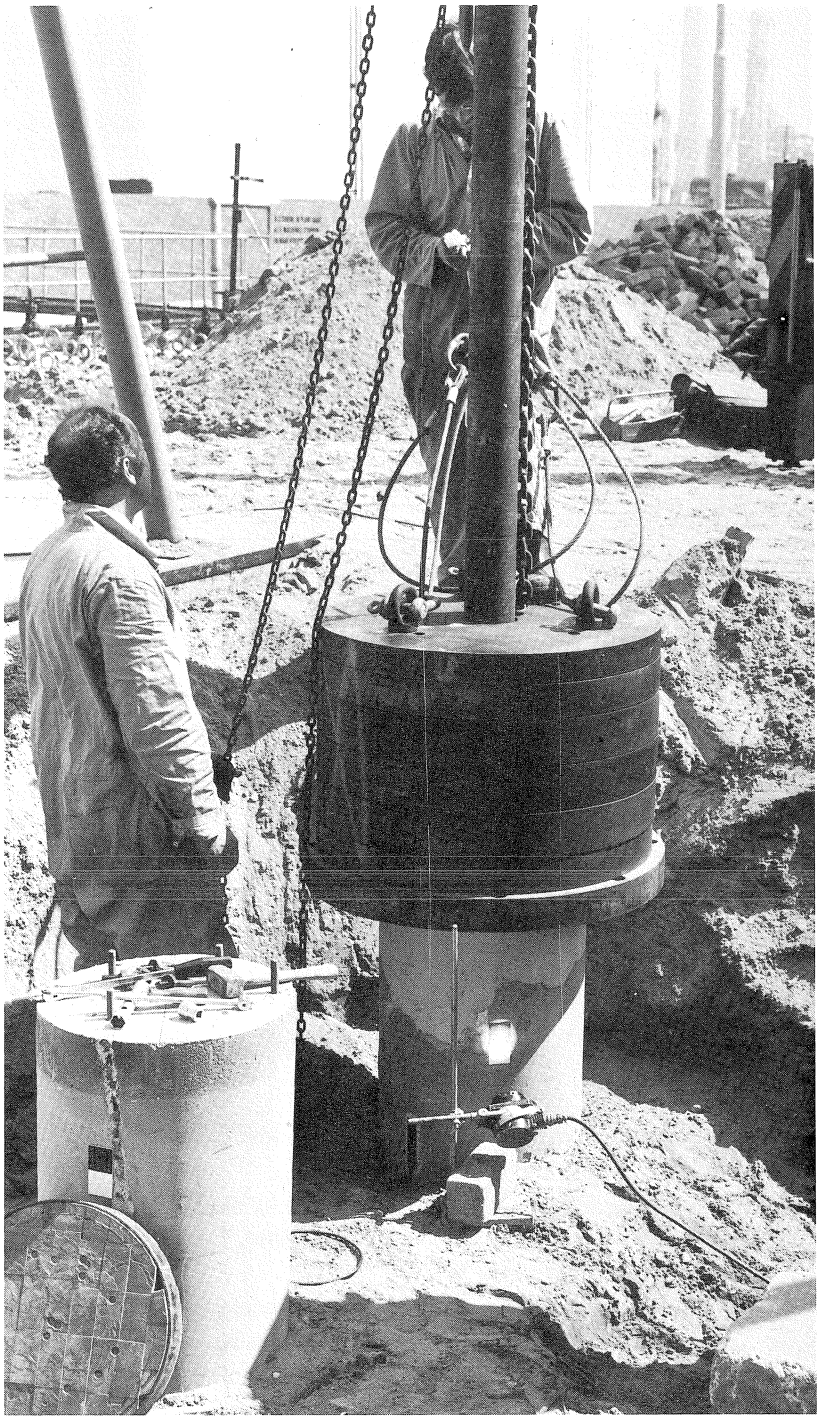

Fig. 25. Drop-weight.

Fig. 26. Pneumatic hammer.

3.4.3 Transport of the equipment

All the necessary equipment to perform a loading test is carried in a van with a trailer.

Also, a generator and cylinders of compressed air are available to make the equipment fully self-sufficient.

3.5 *Computer test results*

The main test results are plotted on an oscilloscope screen after the computer has analysed the results of the measurements.

The results are recorded with a Polaroid camera and presented as four photographs.

Photograph 1 (see Fig. 27) represents the unscaled strain and displacement signals.

In photograph 2 (see Fig. 28) the signals are scaled and the measured strain signal is converted to a force signal.

Photograph 3 (see Fig. 29) is the first result of the analysis. The upper part of the photograph represents the measured force (solid line) and the differentiated displacement signal (velocity) times impedance (dashed line). The lower part of the photograph represents the skin friction along the pile shaft, which can be calculated from the difference between measured force and velocity times impedance.

Photograph 4 (see Fig. 30) is the most important result. It shows the calculated static load-displacement curve.

The working load of the tested foundation pile can be deduced from this photograph.

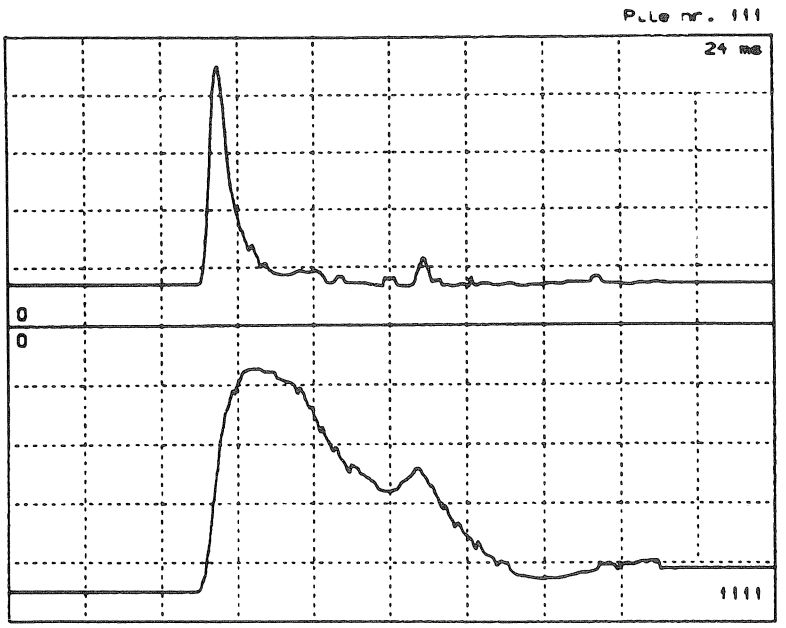

Fig. 27. Signals of strain and displacement.

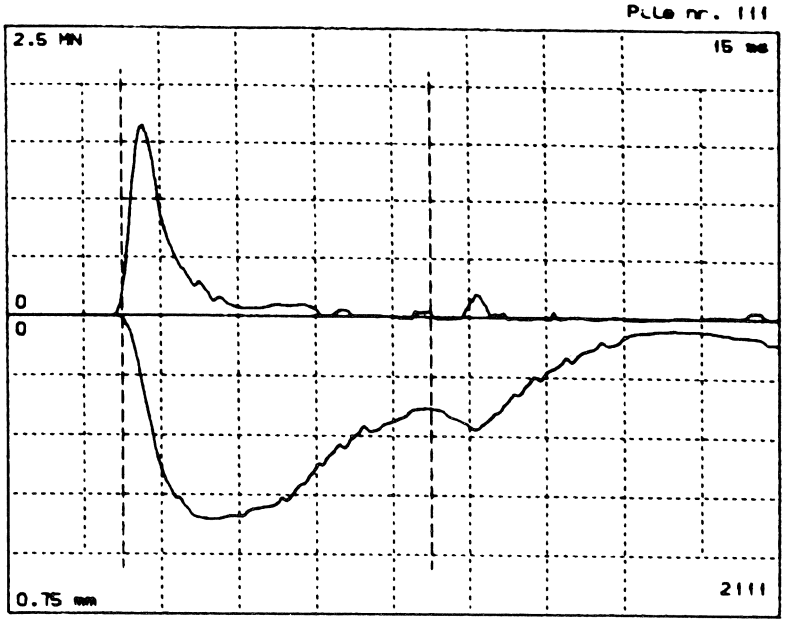

Fig. 28. Forces and displacements.

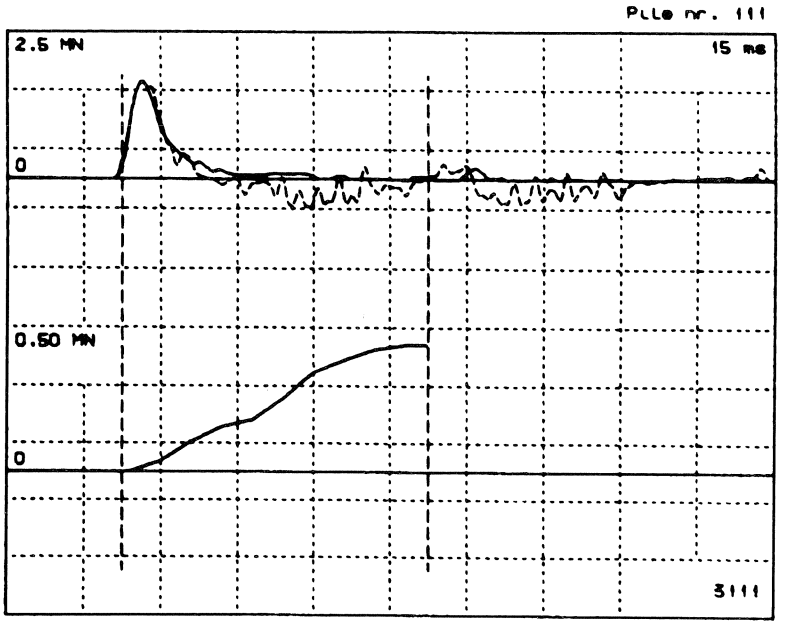

Fig. 29. Upper curves: forces, strains and velocities; lower curve: skin friction.

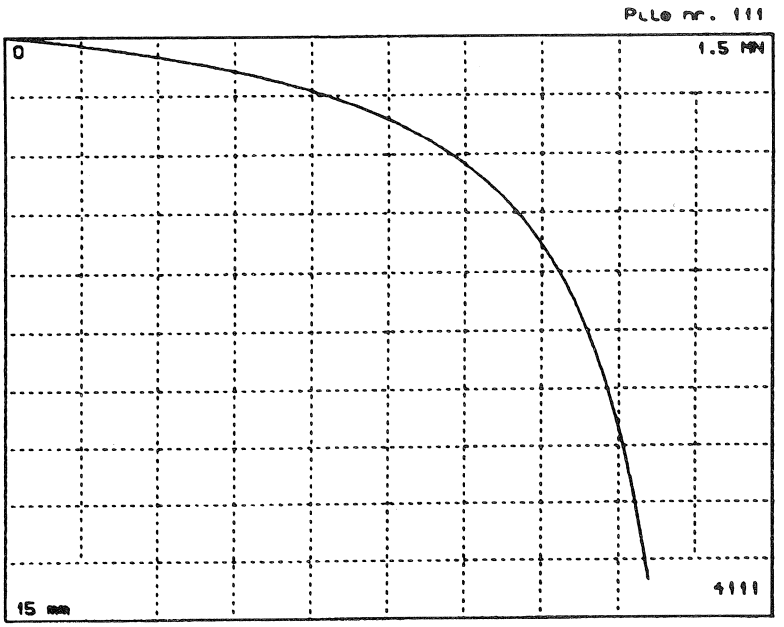

Fig. 30. Load-displacement diagram.

4 Case histories

4.1 *Introduction*

Experience extending over a period of 20 years (up to 1981) with the integrity test and 6 years with the load test has yielded a large number of cases, both onshore and offshore.

Driven piles as well as cast-in-situ piles of a great many systems have been tested. Some of those cases will be examined here in order, to indicate the possibilities of TNO pile testing.

The first case history deals with the statistical treatment of load test results. This is followed by case histories for driven and cast-in-situ piles.

4.2 *Statistical treatment of load test results*

By subjecting all the piles in a site to the integrity test a good impression of the quality of integrity of the piles is obtained.

The integrity tests give information concerning cracks, local increases or decreases in cross section, and pile length, as well as some indication of the skin friction. The results of these integrity tests contain enough information to pick out those piles which have the lowest bearing capacity.

Dynamic bearing capacity tests can be performed on these selected piles. The results of these tests can then be analysed statistically.

For example, this can be done by establishing a statistical distribution $p(n)$ of the safety factor (n), which will be defined as:

$$n = \frac{F_{tot}}{F_w}$$

where:

F_{tot} = total bearing capacity
F_w = working load

The minimum bearing capacity (F_{min}) that could occur is found by using the Student's t-tests:

$$F_{min} = F_{mean} - t\sigma\sqrt{1 + \frac{1}{m}}$$

where:

m = number of bearing capacity tests
F_{mean} = mean value of the m total bearing capacity values (F_{tot})
σ = standaard deviation of the m-tests
t = variable of Student's t-distribution

Values for t are tabulated, for example by Kreysig [5], as a function of the number of degrees of freedom $(m-1)$ and the accepted probability that F_{tot} could be less than F_{min}.

An example of the calculation of F_{min} is now given.

On a building site 36 foundation piles were selected, from a total of 200 piles, for a bearing capacity test.

The piles were installed by driving a 13 m long steel tube (Ø 430 mm) into the ground. After being filled with concrete, the tube was extracted. A steel plate, positioned under the pile toe, remained in the ground. The pile dimensions were designed for an ultimate bearing capacity of approximately 1 MN and a working load of 0.5 MN.

The minimum value of the safety factors obtained was 1.87, the mean value 3.40, and the standard deviation 1.02.

By grouping the safety factors it was possible to plot a histogram, which is given in Fig. 31.

The distribution can be approximated by a Weibull distribution with $n = 1.8$ as the zero point.

A typical load deflection curve for one of the tested piles is given in Fig. 32.

The minimum bearing capacity (F_{min}) was found by using only three test piles and applying Student's t-test:

$$F_{min} = F_{mean} - \frac{2.92}{3}\sqrt{\frac{\Sigma(F - F_{mean})^2}{2}}$$

$$F_{mean} - 2.92\sigma\sqrt{\frac{1}{3} + \frac{1}{p}}$$

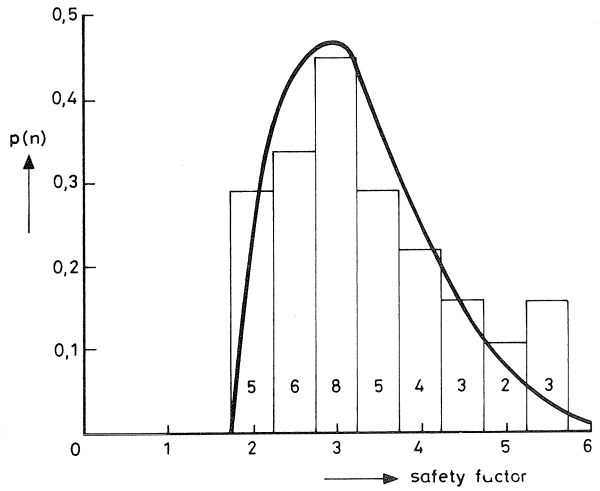

Fig. 31. Weibull distribution and histogram.

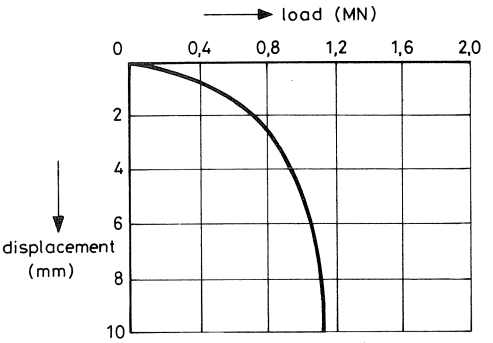

Fig. 32. Load-displacement diagram.

4.3 *Case history of an integrity test performed on cast-in-situ piles*

Fig. 33 shows three photographs, representing some of the results of an integrity test performed on cast-in-situ piles on a site in the province of Brabant, The Netherlands.

In the upper and lower part of the first photograph, the test results of two piles have been taken combined.

The first peak in the signal is caused by the hammer blow; the second smaller peak is the reflex of a decrease in cross-section, in this case the pile toe.

This smaller peak appears 4 milliseconds after the start of the blow, which, assuming a wave velocity of 4000 m/s (in concrete), denotes a pile length of 8 m.

The actual length of the pile had been stated to be 8 m.

The reflex of the toe, although rather small in this case because of heavy skin friction, appears at the right moment.

Because no reflex of decreases in cross-section could be detected between the start of the blow and the reflex of the toe, the integrity of the pile is rated as reliable.

The second photograph of Fig. 33 shows a peak occuring 1.5 milliseconds (3 m) after the start of the blow, this peak being caused by a decrease in cross-section. A repeat of this peak can be observed furtheron in the signal and means that the wave introduced by the blow is travelling between the pile top and the decrease in cross-section.

Because no information is obtained from the pile toe, this pile is rated as unreliable.

The third photograph indicates a small peak 1.5 ms (3 m) after the blow and a stronger one after 2.5 milliseconds (5 m).

So a decrease in cross-section at 3 m and a more pronounced one at 5 m from the pile top can be expected.

After the first part a repeat of the signal can be observed and no information about the pile toe is obtained. This pile, too, is rated as unreliable.

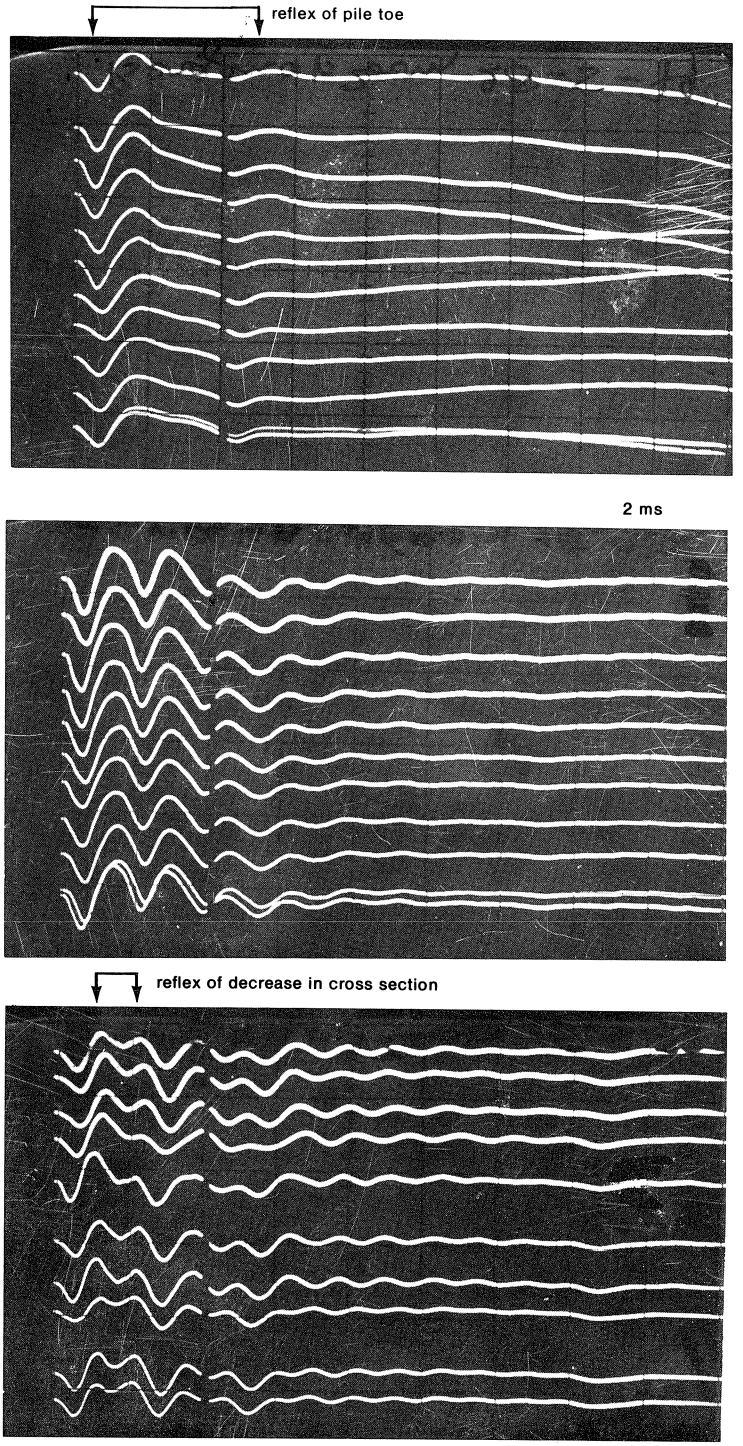

Fig. 33. Integrity test results.

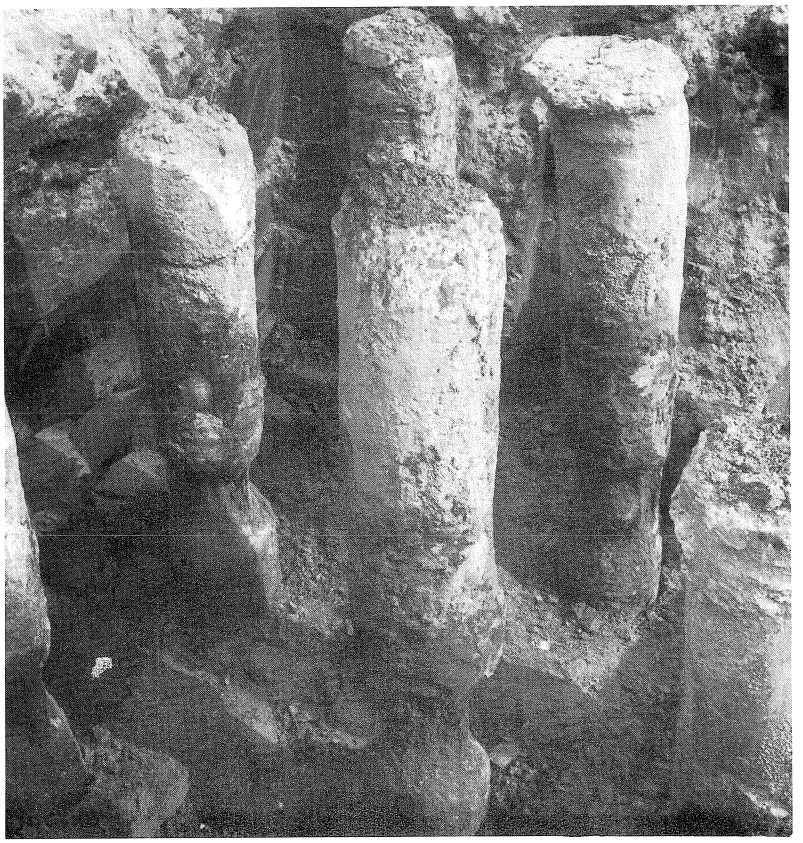

Fig. 34. Excavated cast-in-situ piles with locally decreased cross-section.

Because a number of piles in a specific area of the site showed results like those in the second and third photograph of Fig. 33, further investigation was advised.

This was done by excavating the piles diagnosed as unreliable, the result of which is shown in Fig. 34, which confirms the results obtained from the integrity test.

The decrease in cross-section turned out to be caused by a locally occuring stratum of clay.

After being repaired, the piles were incorporated in the foundation structure.

4.4 *Case history of a driven pile*

Fig. 35 shows the results obtained from an integrity test performed on a prestressed driven pile (length 22 m, cross-section 0.16 m^2) on a site in the province of North Holland.

Because the reflex of the toe appears 11 milliseconds after the start of the blow (22 m from the pile top), which corresponds to the stated pile lentgh, the integrity of the pile is rated as reliable.

For further research a dynamic bearing capacity and static bearing capacity test were performed on this pile.

The recorded signals of the dynamic bearing capacity test are shown in Fig. 36. They represent the force and displacement near the pile top, caused by the impact of a weight of 1200 kg falling from a height of 1.5 m.

Five typical parts can be distinguished in the signals.

Part 1 of the signals represents the impact force, with a maximum of 3.89 MN, and the elastic compression of the pile, with a sion of the pile, with a maximum of 4 mm.

The influence of the forces acting along the pile shaft (the pile is pushed upwards) is revealed in part 2.

From this part of the signals the skin friction acting along the shaft can be deduced, by determining the difference between the impact force (solid line) and the velocity times impedance (dashed line) (see Fig. 37).

The calculated skin friction along the pile shaft is also given in this diagram. It starts at a level of 4 m from the pile top and reaches a maximum of 0.75 MN at 16 m.

In part 3 of the signal, a downward ,movement caused by a reflected tension wave of the pile toe can be observed.

The recording of a tension wave, 0.4 MN in this case, means that the downward compression wave caused by the impact force, reduced by the forces acting along the pile shaft, could not be fully transferred to the soil below the pile toe. The non-transferred part is reflected as a tension wave. So with the results now obtained, such as impact force, skin friction and reflected tension wave, the toe resistance can be calculated: in this case it is found to be 2.73 MN.

Part 4 represents the dying-out of the stresses and movements of the pile. From this part the spring stiffness of the soil can be determined because the combination of pile and soil can be considered in this part as a damped single-freedom system.

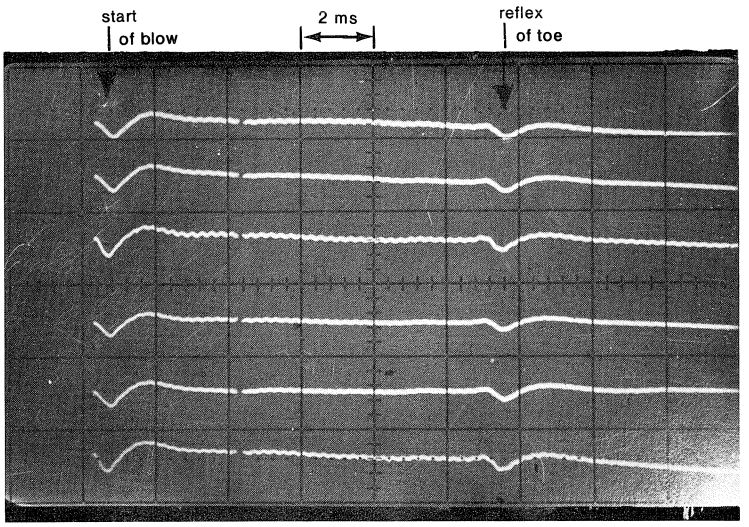

Fig. 35. Integrity test result for a driven pile.

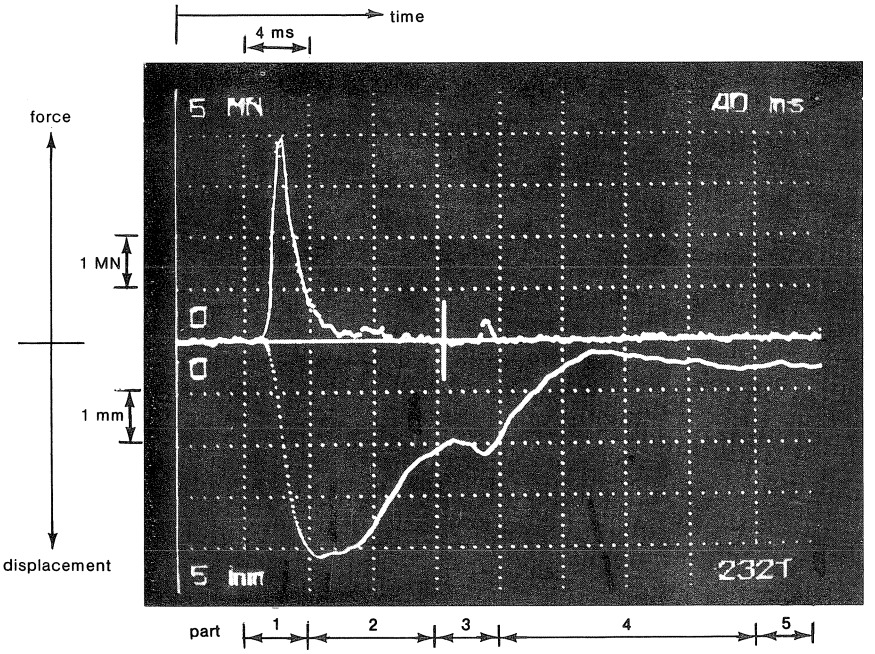

Fig. 36. Force and displacement measured near the top of a driven pile.

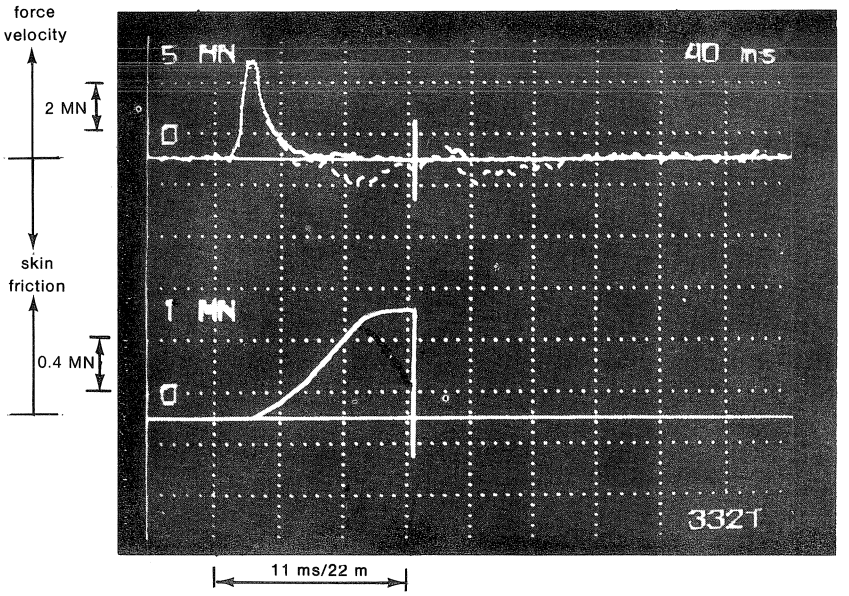

Fig. 37. Force and velocity × impedance and calculated skin friction along the pile shaft.

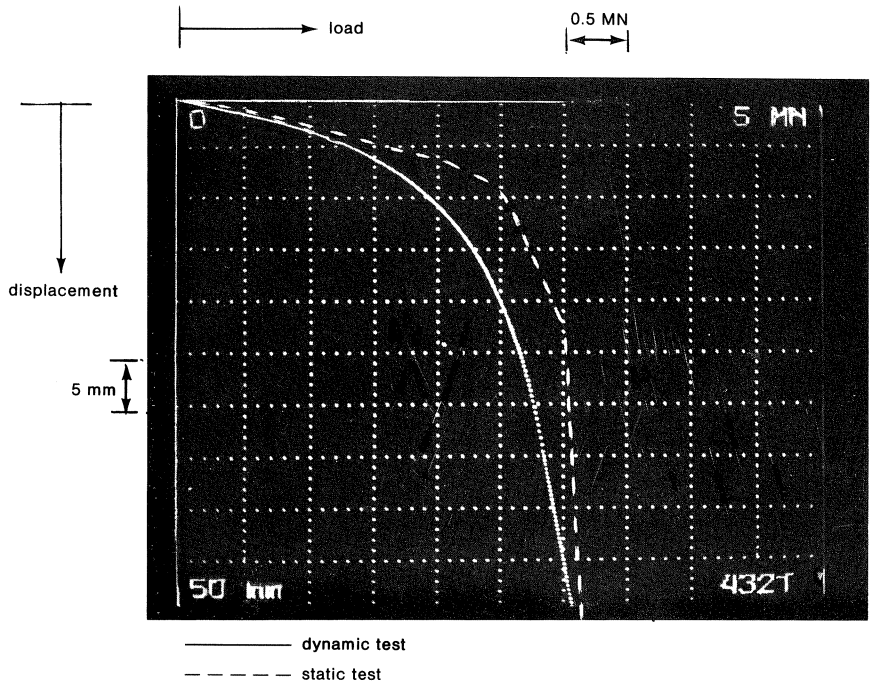

Fig. 38. Load-displacement diagram.

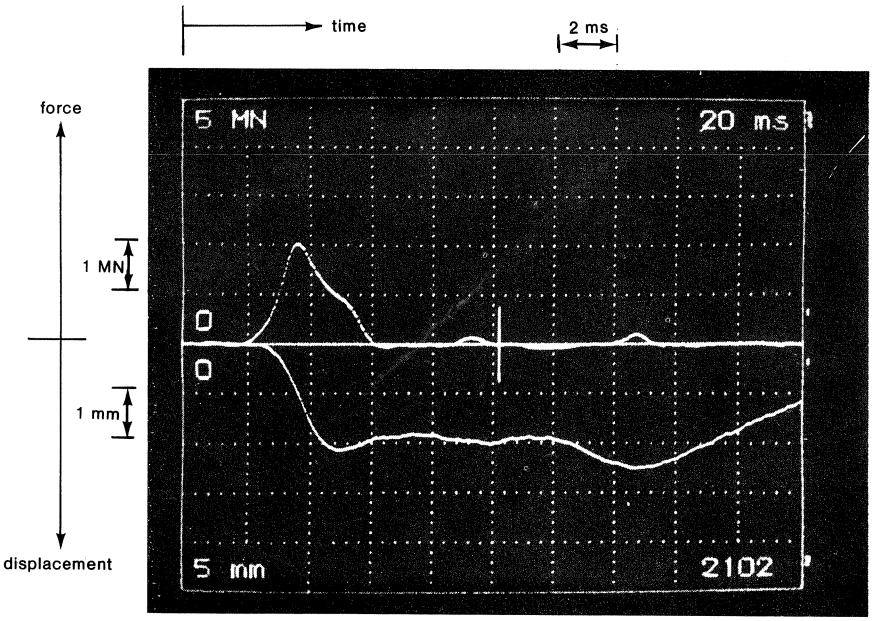

Fig. 39. Force and displacement measured near the top of a cast-in-situ pile.

In part 5 of the signal the remaining settlement of the pile after the impact, in this case (0.5 mm), can be observed. It contains information about the attainment of the bearing capacity of the pile.

With the results obtained from the various parts of the signals, such as skin friction, toe resistance and the spring stiffness of the soil, a load-displacement diagram can be plotted (see Fig. 38).

The total or ultimate bearing capacity equals the sum of skin friction and toe resistance and is, for this case, 3.48 MN. For comparison the result obtained from the static load test, with an ultimate bearing capacity of 3.65 MN, has been included (dashed line).

Up to 1.5 MN there is satisfactory agreement between the static load-displacement diagram and the diagram calculated from the dynamic results, but then a deviation occurs. Nevertheless, the ultimate bearing capacity and the most important part of the load displacement diagram, the practical load being 1.5 MN, have been well predicted.

4.5 *Case history of a bearing capacity test performed on a cast-in-situ pile*

Fig. 39 shows the recorded signals of a bearing capacity test performed on a cast-in-situ pile (length 15.85 m, cross-section 0.1385 m^2) on a site at Delft, The Netherlands.

Just as in the case of a driven pile, the five typical parts can be distinguished in the signals. Initially the signals were processed in the same way as those or a smooth driven pile.

The calculation result was an ultimate bearing capacity of 2.57 MN, split-up into 1.36 MN skin friction and 1.08 MN toe resistance.

This dynamic bearing capacity result seemed too high compared with the static bearing capacity test, which indicated an ultimate bearing capacity of 2.08 MN, while al-

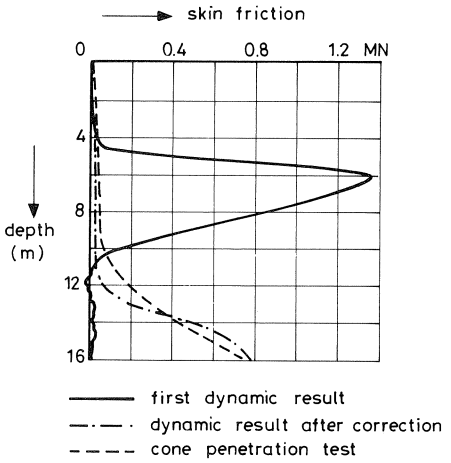

Fig. 40. Skin friction calculated from dynamic results and cone penetration test.

so the agreement with the skin friction (0.90 MN) and toe resistance (1.24 MN) calculated from a cone penetration test was rather poor (see Fig. 40).

The maximum skin friction of the dynamic bearing capacity test occurred at a level where only soft peat layers were present. This disagreement was solved by bringing the shape of the pile into the calculations.

If a downward compression wave, introduced by the impact of a falling weight, meets an enlargement in cross-section, a part of this wave will be reflected. This reflected compression wave introduces an upward movement into the pile in the same way that skin friction manifests itself.

In the case of a reduction in cross-section a tension wave, ontroducing a downward movement into the pile, is reflected back.

So the information about the forces acting along the pile shaft is disturbed by reflected waves generated by changes in shape. If information about the shape of the pile is available, these disturbances due to reflected waves can be eliminated in the recorded signals.

In this case there was hardly any skin friction in the upper soil layers, and the enlargement could be estimated quite satisfactorily from the ratio between the maximum of the compression wave introduced by the impact and the reflected compression wave. Fig. 41 represents the force and velocity times impedance recorded at the same level near the pile top.

This exemple has been taken because the waves travelling upwards, caused by reflections at shape changes or by forces acting along the pile shaft, can be deduced from the difference between these signals. It can be seen that 2 milliseconds after the start of the blow (4 m from the pile top) deviation between force and velocity occurs. Because skin friction is not likely at this depth, it can be assumed that an enlargement in pile cross-

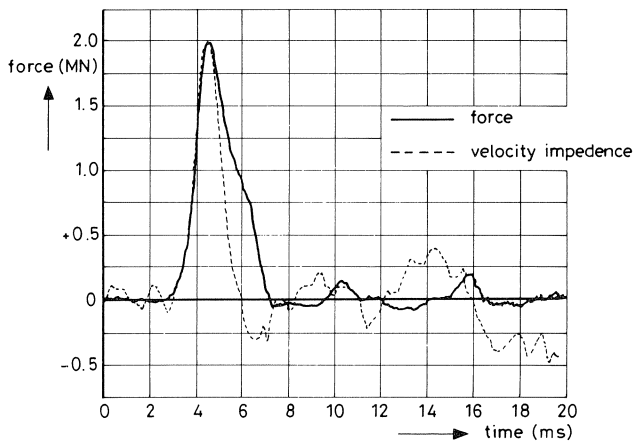

Fig. 41. Force and velocity × impedance.

section starts at this level.

The deviation reaches a maximum after 4 milliseconds (8 m from the top), while after 6 milliseconds (12 m from the top) the reflection of a tension wave, caused by a reduction in cross-section, can be observed. With these results the pile shape was estimated, and the influence of shape changes eliminated.

The estimated pile shape was in good agreement with the recorded amounts of concrete consumed at different levels during the installing of the pile.

The corrected signals of force and velocity together with the estimated pile form are shown in Fig. 42. The signals "coincide" now over the first 6 milliseconds and satisfy the

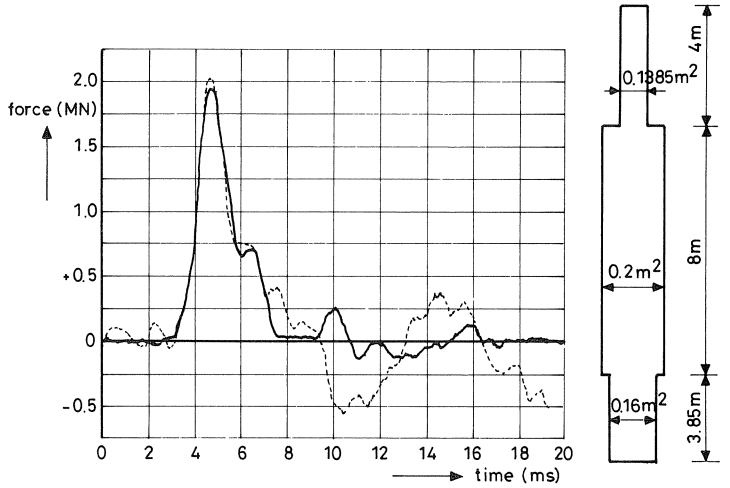

Fig. 42. Corrected force and velocity × impedance and assumed pile shape.

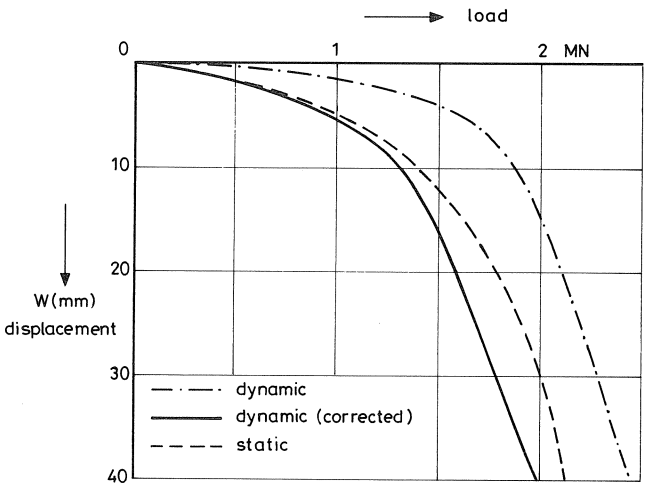

Fig. 43. Load displacement diagrams obtained from static and dynamic results.

assumption of less skin friction in the upper layers, while near the pile toe the influence of skin friction, originally hidden in the signals, now appears. The skin friction now obtained is shown as a dashed line in Fig. 40.

With these newly obtained results a fresh comparison between dynamic bearing capacity test (1.98 MN) and static bearing capacity test (2.08 MN) was made, as shown in Fig. 43.

The agreement between the load displacement diagrams obtained from static and from dynamic results is now satisfactory.

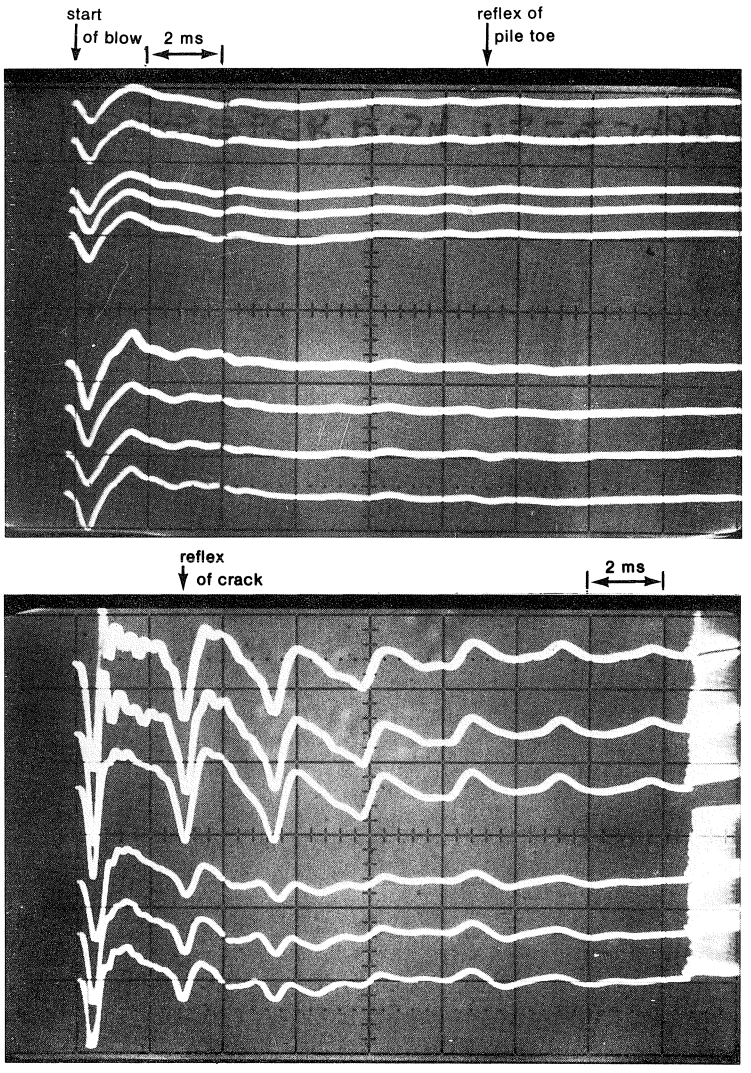

Fig. 44. Integrity test results of cast-in-situ piles.

4.6 *Case history of a defective cast-in-situ pile*

Fig. 44 represents some integrity test results obtained from a building site near The Hague.

In the upper and lower part of the first photograph the results of two piles are combined.

A reflection of the appears after 12 milliseconds (26 m from the pile top), which agrees with the stated lengths. As they satisfy the requirements for good integrity, these piles are rated as reliable.

In the second photograph the test results of two piles have likewise been combined. The signals give sharp reflections after 3 milliseconds (6 m from the pile top), indicating the presence of cracks at this level.

Because no reflection from the toe was obtained, these piles appeared suspect, and a further investigation of their quality was advised. They were not rejected immediately, because a pile with a horizontal rather flat cracked area is well able to transfer a vertical compression load.

The dynamic bearing capacity test was chosen as the method for further investigation. The first photograph in Fig. 45 shows the force and displacement signals recorded during the first impact on one of the cracked piles. The impact force was introduced by dropping a mass of 1200 kg from a height of 0.25 m on the top of the pile.

The vertical signal in the middle of Fig. 45 indicates the place where the reflection of the pile toe is expected, while the dashed line represents the remaining settlement of the top of the pile after the impact. The presence of the crack manifests itself very well in the displacement signal, because after completion of the blow the top of the pile continues to move downwards.

In a pile of good integrity, the top of the pile would, after the elastic compression under the blow, at least remain in the same position or move upwards because of skin friction.

To determine the force transfer in the cracked zone the part of the pile above the crack was considered as a pile of 6 m length, for which the "toe" resistance had to be determined. For the first impact the calculated result of the "toe" resistance was 1.22 MN.

The other two photographs in Fig. 45 show the results if successive impacts, and it appears that the toe resistance increases, while the remaining settlement decreases. The increasing resistance (spring stiffness) in the cracked zone manifests itself also in the upward movement of the pile top after the impact.

After the first blow the top of the pile remains more or less at the same level, while after several impacts it starts to move upwards faster and faster.

The last test, the seventh impact, yielded a "toe" resistance of 2.22 MN.

The tests were stopped, because if had by then been estiblished that force transfer in the cracked zone was effective and safe enough to allow the pile to be used under the actual load of 1 MN.

As the cracked parts of the pile were driven one upon the other, an initial settlement, equalling the crack width, could also be prevented.

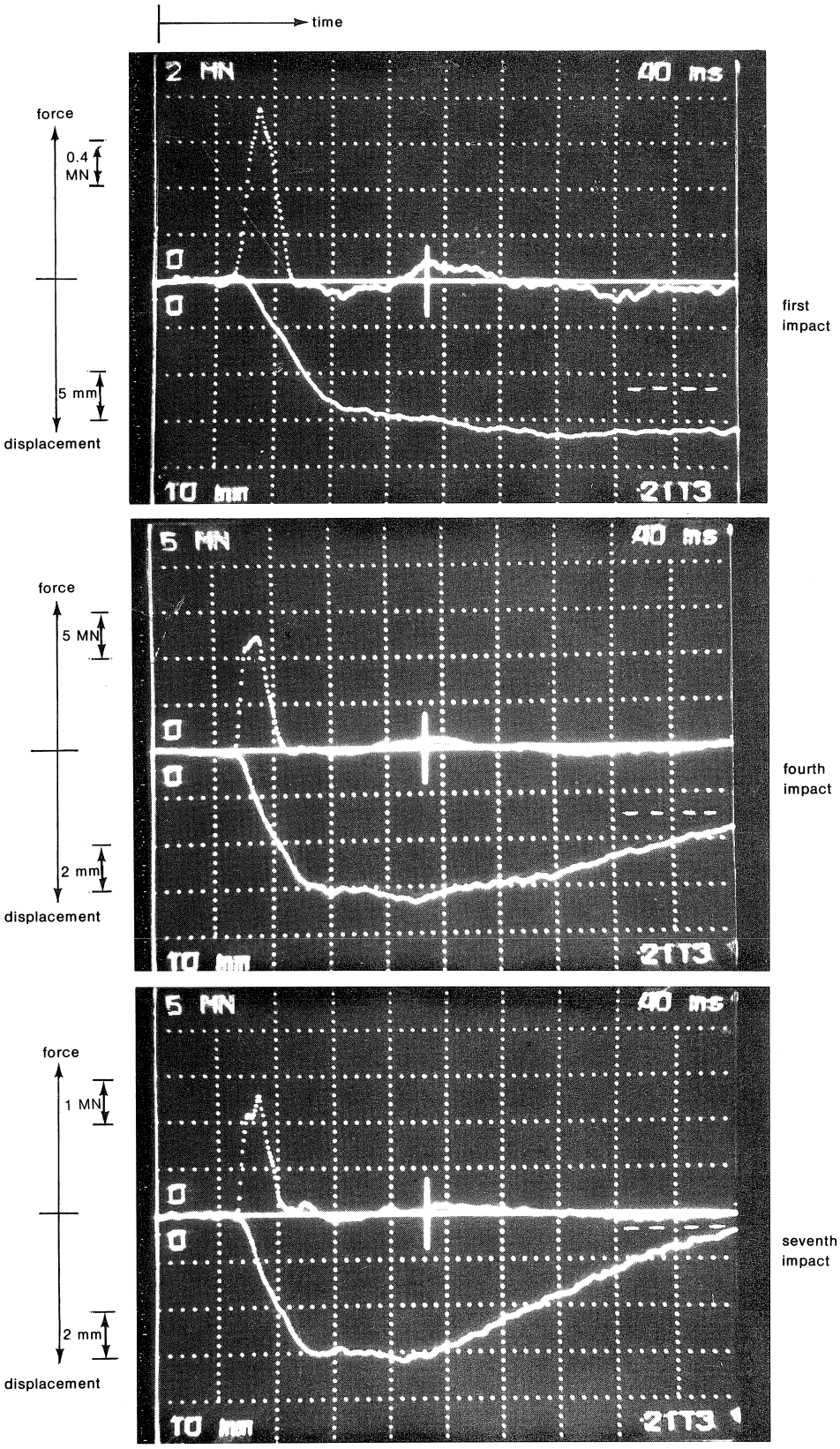

Fig. 45. Force and displacement signals for several impacts.

5 Concluding remarks

The combination of theory and much practical experience with the integrity test and dynamic load test has yielded methods for the determination of the safety of a pile foundation.

Pile length, cross-sectional reductions and other dicontinuities can be determined with the integrity test.

The static load behaviour, skin friction and toe resistance can be determined by means of the dynamic load test.

The methods of testing have been developed in such a way that their results are immediately available, enabling unnecessary delay on the building site to be avoided.

6 References

1. ALLEN, J. H. and U. DAYAL, The effect of penetration rate on the strength of remolded clay and sand samples. Can. Geotech. J. Vol. 12 (1975)
2. VAN KOTEN, H., MIDDENDORP, P. and VAN BREDERODE, P. J., Analysis of dissipative wave propagation in a pile. Int. Seminar on the Application of Stress Wave Theory on Piles, Stockholm, 1980.
3. DE JOSSELING DE JONG, What is happening in the soil during pile driving. De Ingenieur No. 25 (1956) (Dutch).
4. HEEREMA, E. P., Relationships between wall friction, displacement velocity and horizontal stress in clay and in sand, for pile driveability analysis. Ground Engineering (1979).
5. KREYSIG, E. Introductory mathematical statistics. Wiley International Edition.
6. LITKONKI, S. and T. J. POSKITT, Damping constants for pile driveability calculations. Géotechnique 30, 1980, No. 1, pp. 77–86.
7. ROLLBERG, D., Die Kraft-Setzungslinie von Pfählen. Bouwingenieur 53 (1978).
8. VOITUS VAN HAMME, G. E. J. S. L. et al., Hydroblok and improved pile driving analysis. De Ingenieur, No. 8, Vol. 86 (1974).